Publication title	Combustion modeling in a pressurized gas turbine burner using Large-Eddy Simulations
Authors	J. M: García-Oliver, J.M. Pastor, I. Olmeda, A. Both, D. Mira
Issue Date	2022
Publisher	XII National and y III International Conference on Engineering Thermodynamics
Type of publication	Conference proceeding
Acknowledgement	The ESTiMatE project has received funding from the Clean Sky 2 Joint Undertaking under the European Union's Horizon 2020 research and innovation programme under grant agreement No 821418.
Disclaimer	

12CNIT-2022 - FULL PAPER

Combustion modeling in a pressurized gas turbine burner using Large-Eddy Simulations

J.M. García-Oliver[1], J.M. Pastor[1], I. Olmeda[1], A. Both[2], D. Mira[2]

[1] CMT-Motores Térmicos, Universitat Politècnica de València, Spain

[2] Barcelona Supercomputing Center (BSC), Spain

Keywords: *Large-Eddy Simulations, Flamelet generated manifolds, Gas turbine burner, Combustion.*

TOPIC: NUMERICAL SIMULATION AND MODELLING

1. Introduction

Due to the health and environmental harmful effects of pollutant emissions, investigation in combustion and particulates generation is an important target for the development of next generation gas turbine burners. Since manufacturing and testing realistic burners in different operating conditions is very expensive, Computational Fluid Dynamics (CFD) methods are a more than viable alternative to address the study of combustion in this type of applications, due to their capability of reducing the time scales and cost. In particular, Large-Eddy Simulation (LES) is a powerful tool for accurately predicting turbulence, reacting flow and soot formation in complex geometries with an affordable computational cost. In this context, it is usual to analyze simplified burners or academic test cases such as turbulent jet flames due to the lack of reliability of experimental measurements under real engine operating conditions.

Thus, the burner recently investigated by Geigle et al. [1][2] at the German Aerospace Center (DLR) is a widely studied model combustor in terms of turbulent combustion and soot formation. It is a pressurized burner with a dual swirler configuration for the primary air supply, generating a strong recirculation region inside the combustion chamber. Secondary air is injected downstream, creating a soot oxidation zone typical of the Rich-Burn/Quick-Quench/Lean-Burn (RQL) combustor concept.

In this work, LES of the pressurized burner developed at DLR have been carried out using a flamelet-based tabulated combustion model. A detailed description of the modeling approach is addressed in Section 2. The experimental test rig and numerical configuration are presented in Section 3. Section 4 includes the analysis of the simulation results. Finally, the work is closed with the main conclusions extracted.

2. Modeling approach

2.1 Governing equations

The equations describing the reacting flow correspond to the low-Mach number approximation of the Navier-Stokes with the energy equation represented by the total enthalpy. A Favre-filtered description of the governing equations is followed to avoid the modelling of terms including density fluctuations. Favre-filtering of any quantity ϕ is denoted by $\tilde{\phi}$, while Reynolds-filtering is given by $\bar{\phi}$. The filtered governing equations for LES correspond to the continuity, momentum and enthalpy and read as:

$$\frac{\partial \bar{\rho}}{\partial t} + \boldsymbol{\nabla} \cdot (\bar{\rho}\tilde{\boldsymbol{u}}) = 0, \tag{1}$$

$$\frac{\partial \bar{\rho}\tilde{\boldsymbol{u}}}{\partial t} + \boldsymbol{\nabla} \cdot (\bar{\rho}\tilde{\boldsymbol{u}}\tilde{\boldsymbol{u}}) = -\boldsymbol{\nabla} \cdot \bar{\tau}_M - \boldsymbol{\nabla}\bar{p} + \boldsymbol{\nabla} \cdot (\bar{\mu}\boldsymbol{\nabla}\tilde{\boldsymbol{u}}), \tag{2}$$

$$\frac{\partial \bar{\rho}\tilde{h}}{\partial t} + \boldsymbol{\nabla} \cdot \left(\bar{\rho}\tilde{\boldsymbol{u}}\tilde{h}\right) = -\boldsymbol{\nabla} \cdot \bar{\tau}_h + \boldsymbol{\nabla} \cdot \left(\bar{\rho}\bar{D}\boldsymbol{\nabla}\tilde{h}\right), \tag{3}$$

where standard notation is used for all the quantities with $\bar{\rho}$, $\tilde{\boldsymbol{u}}$, $\tilde{h}$, $\bar{D}$, $\bar{p}$ and $\bar{\mu}$ represent the density, velocity vector, total enthalpy (sensible and chemical), diffusivity, pressure and dynamic viscosity using filtered quantities. The τ term stands for the unresolved or subgrid terms related to the filtering operation and applies to the unresolved momentum flux $\bar{\tau}_M$ and the unresolved enthalpy flux $\bar{\tau}_h$. The subgrid viscous stress tensor is determined based on the Stokes' assumption and the turbulence contribution is obtained by the use of the Boussinesq approximation [ref]. A unity Lewis number assumption has been made to simplify the scalar transport in the governing equations. Heating due to viscous forces is neglected in the enthalpy equation and the unresolved heat flux is modelled using a gradient diffusion approach [ref]. The modelling framework is closed by an appropriate expression for the subgrid-scale viscosity, obtained from the Vreman [4] model.

The equations are solved by the multiphysics code Alya [5]. The discretization strategy is based on a conservative finite element convective scheme [6], where stabilization is only introduced for the continuity equation by means of a non-incremental fractional-step method. Standard stabilized finite elements are used for the scalars, while the time integration is carried out by means of an explicit third order Runge-Kutta scheme for momentum and scalars.

2.2 Turbulent combustion model

The combustion and thermo-chemical state of this burner is described by the flamelet method [7]. A scale separation between the flow and the chemistry is assumed, so that the flame structure can be defined by a composition of one-dimensional (1D) flames. In order to account for strain effects on the thermodiffusive behavior of the reacting layer, laminar diffusion flamelets at different strain rates are tabulated until the extinction point is encountered. An extinguishing flamelet initiated from the last stable instance (extinction point) is used as a natural continuation of this two-dimensional manifold [8], conducting an unsteady calculation to account the transient development of the thermochemical state.

The chemistry for ethylene is given by a 214-species and 1537 reactions mechanism developed in [9], and the flamelet equations are solved in physical space with the chem1d code [10] using a unity Lewis number approach.

The effects of heat loss on the flamelet database are considered by the tabulation of strained diffusion flames at different enthalpy levels. The local enthalpy deficit is generated through a radiative source term in the energy equation without changing the inlet temperature of the reactants. The enthalpy level of the mixture can be characterized by the scale enthalpy $\tilde{\imath}$, which is computed from the transport of total enthalpy $\tilde{h}$ as:

$$\tilde{\imath} = \frac{\tilde{h} - h_{min}}{h_{max} - h_{min}}, \tag{4}$$

This enthalpy scaling is defined by the maximum and minimum enthalpy levels, h_{max} and h_{min} given in the low-dimensional manifold for each mixture fraction and reaction progress. Different enthalpy levels are reached by the scaling of the radiative term (f_{rad}).

Three controlling variables are used to characterize the thermochemical state of the flamelets composing the manifold: mixture fraction Z, progress variable Y_c, and normalized enthalpy i. The mixture fraction is determined by Bilger's formula, while the progress variable Y_c in our study is defined as:

$$Y_c = \sum_{k=1}^{N} \frac{a_k}{W_k} Y_k, \tag{5}$$

with $N = 6$ using $Y_k = \{Y_{CO_2}, Y_{CO}, Y_{H_2}, Y_{H_2O}, Y_{A4}, Y_{O2}\}$, and W_k being the molar weight of the chemical species. The contribution of each species to the progress variable Y_k is given by the coefficients $a_k = \{1, 1, 0.35, 1, 20, -0.01\}$ respectively.

Transport equations for the filtered controlling variables $\tilde{Z}$ and $\widetilde{Y_c}$ are defined in order to describe the chemical evolution of the reacting flow, as the normalize enthalpy $\tilde{\imath}$ is obtained directly from the enthalpy, see Eqs. (3) and (4). The system of equations read:

$$\frac{\partial \overline{\rho}\tilde{Z}}{\partial t} + \boldsymbol{\nabla} \cdot \left(\overline{\rho}\widetilde{\boldsymbol{u}}\tilde{Z}\right) = -\boldsymbol{\nabla} \cdot \overline{\tau}_Z + \boldsymbol{\nabla} \cdot \left(\overline{\rho}\overline{D}\boldsymbol{\nabla}\tilde{Z}\right), \tag{6}$$

$$\frac{\partial \overline{\rho}\widetilde{Y_c}}{\partial t} + \boldsymbol{\nabla} \cdot \left(\overline{\rho}\widetilde{\boldsymbol{u}}\widetilde{Y_c}\right) = -\boldsymbol{\nabla} \cdot \overline{\tau}_{Y_c} + \boldsymbol{\nabla} \cdot \left(\overline{\rho}\overline{D}\boldsymbol{\nabla}\widetilde{Y_c}\right) + \overline{\dot{\omega}}_{Y_c}, \tag{7}$$

As for the Navier-Stokes equations, Eqs. (1) to (3), the unresolved terms appearing after the LES filtering $\overline{\tau}_Z$ and $\overline{\tau}_{Y_c}$ are closed using a gradient diffusion approach and $\overline{\dot{\omega}}_{Y_c}$ is the filtered progress variable source term.

In order to account for turbulent-chemistry interactions at the subgrid scale, the tabulated properties ψ from the manifold are integrated with a presumed-shape probability density function (PDF) that

describes the statistical effect of turbulence on the flame structure [10]. To facilitate the flamelet manifold tabulation, retrieval and integration, a scaled progress variable C is then defined as:

$$C = \frac{Y_c - Y_{c,min}}{Y_{c,max} - Y_{c,min}}, \tag{8}$$

Therefore, this three-dimensional manifold $\psi = \psi(\mathrm{Z}, \mathrm{C}, \mathrm{i})$ must be integrated with a filtered joint-PDF. Due to the complexity of considering three independent variables, the joint-PDF is usually treated as a product of statistically independent PDFs of each degree of freedom [12] and the integration of the manifold read as:

$$\widetilde{\psi}(Z, C, i) = \int_0^1 \int_0^1 \int_0^1 \psi(Z, C, i)\tilde{P}(Z)\tilde{P}(C)\tilde{P}(i)dZdCdi, \tag{9}$$

In the present non-premixed turbulent combustion model, presumed shape PDFs are employed in each controlling variable. Both mixture fraction and scaled progress variable distributions are characterized by β-functions, defined by the filtered values from Eqs. (6-8) and subgrid variances, derived from transport equations as described in [13]. Meanwhile a δ-function is applied to the enthalpy parameter. This modelling strategy assumes that most unresolved effects are attributed to spatial mixture fraction and progress variable fluctuations.

3. Test case description

3.1 Experimental setup

The pressurized ethylene-based model combustor investigated at DLR is studied in this work. It exhibits features similar to real gas turbine burners and it is representative of the RQL concept. A more detailed description of the experimental setup can be found in the work of Geigle et al. [1].

A sketch of the geometrical burner characteristics can be observed in Fig. 1 while the two main operating conditions are presented in Table 1. The burner presents a dual radial swirler configuration for air supply. The inner swirler consists of 8 vanes while the outer one is composed of 11 ducts. The combustion chamber has a square section of 68 x 68 mm^2 and a height of 120 mm. Several quartz windows are arranged on the sides of the chamber ensuring the optical access for measurements. Additional ducts for secondary oxidation air injection are located at the corners of the chamber, 80 mm downstream the chamber inlet plane. Fuel is injected through a concentric ring of 60 equally spaced ports located between the inner and outer air inlets.

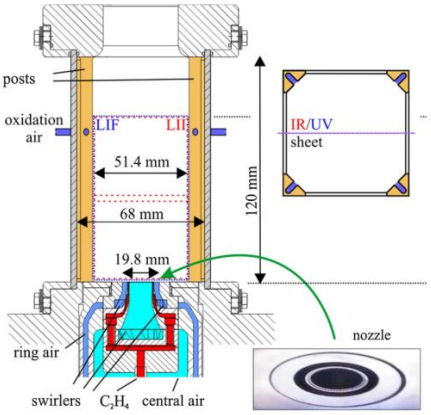

Figure 1. Sketch of DLR burner.

	p (bar)	$\boldsymbol{\phi}$ (-)	$\boldsymbol{Q_{a,c}}$ (slpm)	$\boldsymbol{Q_{a,ox}}$ (slpm)	$\boldsymbol{T_a}$ (K)	$\boldsymbol{Q_f}$ (slpm)	$\boldsymbol{T_f}$ (K)
Op. 1	3	1.2	140.8	187.4	300	39.3	300
Op. 2	3	1.2	140.8	0	300	39.3	300

Table 1. Operating conditions of the DLR burner.

Multiple experimental diagnostics are available at several operating points for flame characterization and soot formation [1][2][3]. Velocity component statistics at different positions inside the combustion chamber were measured using Stereo-Particle Image Velocimetry (Stereo-PIV). Temperature measurements were obtained from Coherent Anti-Stokes Raman scattering (CARS) and OH radical distribution was qualitatively estimated by Laser Induced Fluorescence (LIF). In addition, Planar Laser-Induced Incandescence (LII) was used to measure the soot volume fraction.

3.2 Numerical setup

The computational domain considered for numerical simulations is based on the experimental test rig described in previous subsection. It includes all the different components of the burner: inlet ducts for air and fuel supply, the dual swirler injection system, the combustion chamber and secondary oxidation air ducts, while the fuel injection is modelled as a single continuous ring. Furthermore, the domain includes a cubic volume of 400 mm side at the exit of the burner to reproduce the atmosphere.

As it is already illustrated in Fig. 1, two operating points are evaluated for this study: Op. 1 including secondary air injection and Op. 2, which does not include these jets. Therefore, two meshes are used for this geometry, resulting in a total of 52M and 46M elements respectively for Op. 1 and Op. 2. Fig. 2 shows a representation of the computational domain (Op. 1) and an overview of the mesh. They are

composed mainly of tetrahedrons, prisms and pyramids and a minimum cell size of 0.15 mm is considered for the refinement of the near mixing region inside the combustion chamber. Layer of prisms are applied in the air and fuel ducts in order to better resolve the boundary layer. Concerning the mesh quality, Pope's criterion [14] is used and over 80% of the turbulent kinetic energy is resolved in almost the entire combustion chamber. Other criteria based on the viscosity ratio [15] were evaluated, achieving a sufficiently good LES resolution. In addition, several meshes with different refinements were used to check grid convergence, however, they did not affect significantly the results.

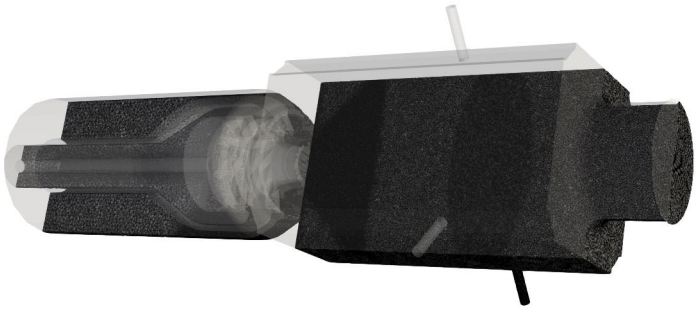

Figure *2*. Computational domain (excluding exit volume) and overview of the mesh.

Constant air and fuel mass flow rates at 300K are prescribed as inlet conditions. Regarding wall boundary conditions, both non-slip adiabatic and isothermal walls are used. A temperature between 700K and 900K is specified for the combustion chamber walls in the isothermal case, according with the experimental measurements.

In this work, time-averages for flow statistics are collected over about 60 ms, which correspond to approximately 3 flow-through times. The flow-through is estimated by the averaged axial velocity integrated over the combustion chamber volume.

4. Results

The following section includes the numerical results of the DLR burner using large-eddy simulations. Results presented in this work are focused on the operating condition considering secondary oxidation air (Op. 1, see Fig. 1). In the first subsection, the assessment of inert and reacting velocity field is performed. An analysis of mixing and combustion processes is addressed in the second subsection, including a comparison between adiabatic and isothermal wall boundary conditions in terms of temperature field.

4.1 Inert and reacting flow assessment

Firstly, the suitability of the CFD model is evaluated by comparing the non-reacting velocity field experimental and numerical results. Flow pattern, turbulent structures inside the combustor, instantaneous and mean axial velocity in the XZ symmetry plane are shown in Fig. 3. This swirl stabilized burner exhibits an inner recirculation zone (IRZ) with negative axial velocities in the central

region, surrounded by the swirled jets (SWJ) with positive axial velocity, and an outer recirculation zone (ORZ) between the SWJ and the side walls. The oxidation side jets (SJ) create a disruption of the axial flow around 80 mm downstream the injection plane, where the radial flow meets. The IRZ is further enhanced upstream this location and the axial flow is accelerated downstream.

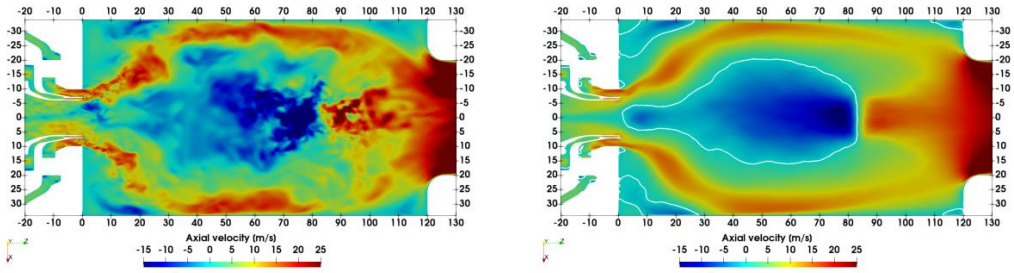

Figure 3. Instantaneous (left) and time-averaged (right) axial velocity from LES of the DLR burner (Op. 1). *White line: zero axial velocity.*

This particular flow behavior can also be observed in different line plots at centerline or radial stations. Fig. 4 and 5 show the comparison between LES and experimental measurements in terms of velocity components for Op. 1 cold flow. Axial velocity is compared at centerline and radial stations in Fig. 4. The recirculation pattern described previously is clearly observed along the burner axis, where axial velocity remains negative until the SJ axial position (80 mm). In addition, the widening of swirled jets is properly captured by LES, as it is observed in radial profiles.

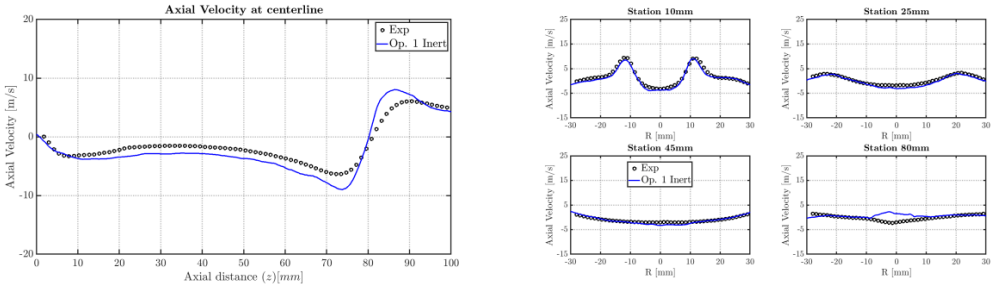

Figure 4. Comparison between LES and experiments for Op. 1 cold flow. Time-averaged axial velocity at centerline (left) and radial stations (right).

Radial and tangential components are compared at radial stations in Fig. 5, where these flow characteristics are also appreciated and well reproduced. Higher discrepancies are found downstream, at 80 mm position, where strong velocity gradients are found due to secondary oxidation ducts. However, the overall agreement between simulation and PIV measurements is satisfactory.

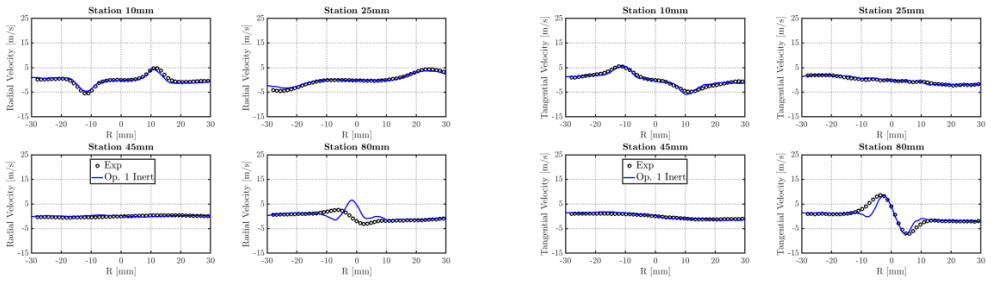

Figure 5. Comparison between LES and experiments for Op. 1 cold flow. Time-averaged radial (left) and tangential (right) velocity components at radial stations.

Regarding the flow field under reacting conditions, Fig. 6 shows the comparison for the Op. 1 combustion case. Similarly, LES can accurately predict the velocity field in most of the combustion chamber. The main difference between the reacting and inert flow fields lies in the velocity magnitude. Combustion results in stronger recirculation regions, reaching an even lower negative velocity peak at centerline. Also, maximum axial velocity values at stations are higher due to the flow expansion.

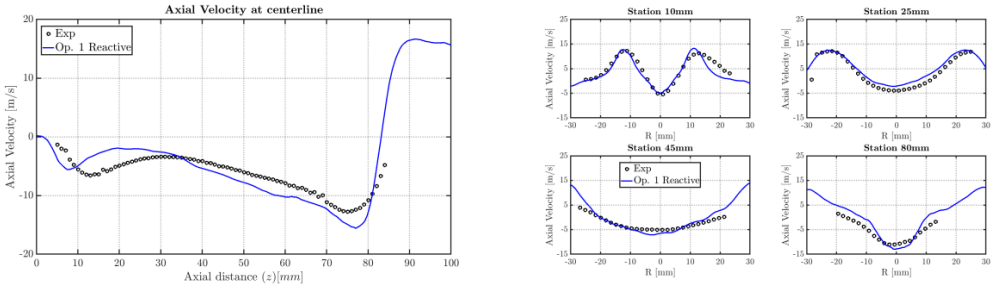

Figure 6. Comparison between LES and experiments for Op. 1 reacting flow. Time-averaged axial velocity at centerline (left) and radial stations (right).

4.2 Mixing and combustion analysis

A qualitative description of the mixing and combustion processes is presented at Fig. 7, where time-averaged mixture fraction and progress variable source term contours are shown in the XZ symmetry plane. In both images, the stoichiometric mixture fraction isoline is remarked in white. It is possible to clearly observe that a fuel rich region develops within the SWJ and that a lean region is found in the IRZ due to the air supplied by the SJ. The Y_c source term contour indicates that the flame is stabilized close to the stoichiometric line surrounding the ORZ and propagates towards richest zones in the SWJ.

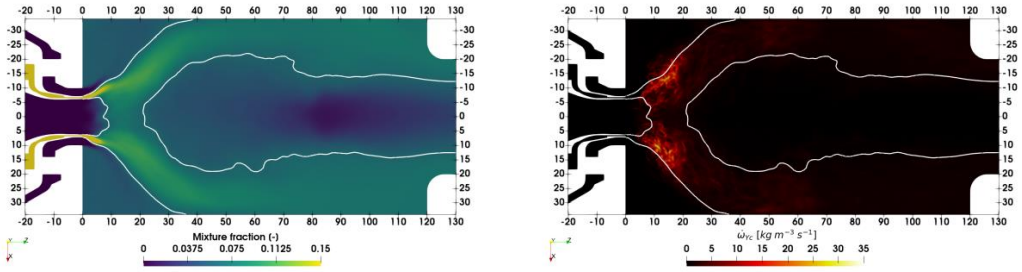

Figure 7. Time-averaged mixture fraction (left) and progress variable source term (right) contours. White line: stoichiometric mixture fraction line.

The impact of including enthalpy losses in the flamelet manifold can be evaluated from Fig. 8. The plots indicate that the temperature prediction at farthest radial positions, closer to the walls, is noticeably improved, especially for the ORZ regions. The effect in the IRZ is negligible except for axial positions close to the SJ, where temperature magnitude is better predicted when including heat losses.

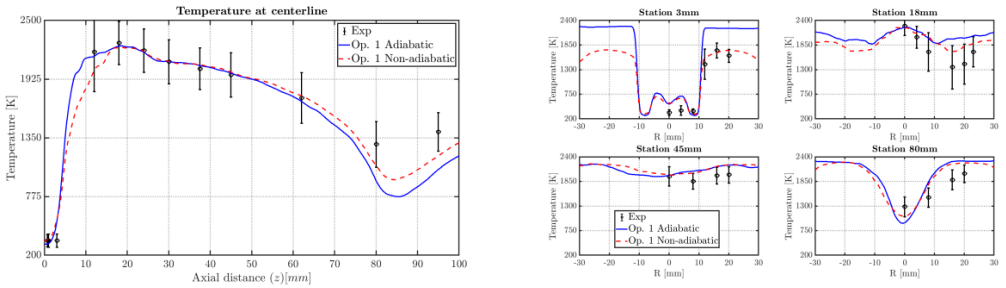

Figure 8. Comparison between LES and experiments for Op. 1 reacting flow. Time-averaged temperature at centerline (left) and radial stations (right).

5. Conclusions

In this work, Large-Eddy Simulations of the DLR pressurized burner have been performed using flamelet-based tabulated chemistry. It has been possible to characterize the cold and reacting flows and evaluate the turbulent combustion model in this type of application. Some discrepancies are found in the region near the secondary injection and further investigation is needed in this issue, but the overall agreement with the experiments is satisfactory and the simulations performed are a good basis for future soot predictions.

Acknowledgements

The research leading to these results has received funding from the European Union's Horizon 2020 Programme under the ESTiMatE project, grant agreement No. 821418. The authors thankfully acknowledge the computer resources at MareNostrum and the technical support provided by Barcelona Supercomputing Center (IM-2020-3-0022, IM-2021-1-0016).

References

[1] K.P. Geigle, R. Hadef, and W. Meier. (2014). Characterization of an Aero-Engine Model Combustor Burning Ethylene at Elevated Pressure." *ASME. J. Eng. Gas Turbines Power*; 136(2): 021505.

[2] K.P. Geigle, M. Köhler, W. O'Loughlin, W. Meier (2015). Investigation of soot formation in pressurized swirl flames by laser measurements of temperature, flame structures and soot concentrations, Proceedings of the Combustion Institute, 35 (3): 3373-3380.

[3] K.P. Geigle, R. Hadef, M. Stöhr, W. Meier (2017). Flow field characterization of pressurized sooting swirl flames and relation to soot distributions, Proceedings of the Combustion Institute, 36(3): 3917-3924.

[4] A. W. Vreman (2004). An eddy-viscosity subgrid-scale model for turbulent shear flow: Algebraic theory and applications, Physics of Fluids 16, 3670-3681.

[5] M. Vázquez et al. (2016), Alya: Multiphysics engineering simulation toward exascale, Journal of Computational Science, 14: 15-27.

[6] A. Both, O. Lehmkuhl, D. Mira, M. Ortega (2020). Low-dissipation finite element strategy for low Mach number reacting flows, Computers & Fluids 200, 104436.

[7] N. Peters (1984). Laminar diffusion flamelet models in non-premixed turbulent combustion, Progress in Energy and Combustion Science, 10(3): 319-339.

[8] S. Delhaye, L.M.T. Somers, J.A. van Oijen, L.P.H. de Goey (2009). Incorporating unsteady flow-effects beyond the extinction limit in flamelet-generated manifolds, Proceedings of the Combustion Institute, 32(1): 1051-1058.

[9] A.Y. Ramirez-Hernandez et al. (2022), Reaction Model Development of Selected Aromatics as Relevant Molecules of a Kerosene Surrogate-The Importance of m-Xylene Within the Combustion of 1,3,5-Trimethylbenzene, Gas Turb. Power, 144(2): 021002.

[10] CHEM1D, A one dimensional flame code, Eindhoven University of Technology, 2002.

[11] P. Domingo, L. Vervisch, D. Veynante (2008). Large-eddy simulation of a lifted methane jet flame in a vitiated coflow, Combustion and Flame, 152(3):415-432.

[12] M. Ihme, H. Pitsch (2008). Prediction of extinction and reignition in nonpremixed turbulent flames using a flamelet/progress variable model: 2. Application in LES of Sandia flames D and E, Combustion and Flame, 155(1-2):90-107.

[13] S. Gövert et al. (2018). The Effect of Partial Premixing and Heat Loss on the Reacting Flow Field Prediction of a Swirl Stabilized Gas Turbine Model Combustor. Flow Turbul. Combust. 100(2): 503-534.

[14] S. Pope (2004). Ten questions concerning the large-eddy simulation of turbulent flows, New J. Phys. 6(35).

[15] I. Celik. Z.N. Cehreli, A. Yavuz (2005). Index of resolution quality for large eddy simulations, J Fluids Eng, Trans ASME, 127 (5): 949-958.